



1 Miocene basement exhumation in the Central Alps recorded  
2 by detrital garnet geochemistry in foreland basin deposits

3 **Laura Stutenbecker<sup>1\*</sup>, Peter M.E. Tollan<sup>2</sup>, Andrea Madella<sup>3</sup>, Pierre Lanari<sup>2</sup>**

4

5 <sup>1</sup>*Institute of Applied Geosciences, Technische Universität Darmstadt, Schnittspahnstr. 9,*  
6 *64287 Darmstadt, Germany*

7 <sup>2</sup>*Institute of Geological Sciences, University of Bern, Baltzerstrasse 1+3, 3012 Bern,*  
8 *Switzerland*

9 <sup>3</sup>*Department of Geosciences, University of Tuebingen, Wilhelmstr. 56, 72074 Tübingen,*  
10 *Germany*

11 \*corresponding author: stutenbecker@geo.tu-darmstadt.de

12 Abstract

13 The Neogene evolution of the European Alps was characterized by the exhumation of crystalline  
14 basement, the so-called external crystalline massifs. Their exhumation presumably controlled the  
15 evolution of relief, distribution of drainage networks and generation of sediment in the Central Alps.  
16 However, due to the absence of suitable proxies, the timing of their surficial exposure, and thus the  
17 initiation of sediment supply from these areas, are poorly constrained.

18 The northern alpine foreland basin preserves the Oligocene to Miocene sedimentary record of tectonic  
19 and climatic adjustments in the hinterland. This contribution analyses the provenance of 25 to 14 My-  
20 old alluvial fan deposits by means of detrital garnet chemistry. Unusually grossular- and spessartine-  
21 rich garnets are found to be unique proxies for identifying detritus from the external crystalline  
22 massifs. In the foreland basin, these garnets are abundant in 14 My-old deposits, thus providing a  
23 minimum age for the surficial exposure of the crystalline basement.



24 1. Introduction

25 Tectonic processes influence the evolution of relief in mountain chains and consequently control the  
26 development of the drainage network, sediment supply and deposition in the foreland basin. The  
27 Central European Alps and their northern foreland basin, formed through the collision of the European  
28 and the Adriatic continents since the Eocene (Schmid et al. 1996, Handy et al. 2010), are a classic  
29 example of such interactions (e.g. Schlunegger et al., 1998; Pfiffner et al., 2002; Vernon et al., 2008,  
30 2009; Baran et al., 2014; Fox et al., 2015). The exhumation of large slices of mid-crustal rocks from  
31 the European plate, the so-called external crystalline massifs, occurred during a late-stage orogenic  
32 event, possibly controlled by crustal delamination in response to lithospheric mantle rollback  
33 (Herwegh et al., 2017). The areas exhumed during this event are today characterized by high relief,  
34 intense glaciation and some of the highest denudation rates measured in the Alps, which all contribute  
35 to their importance as a sediment source (Kühni and Pfiffner, 2001; Wittmann et al., 2007;  
36 Stutenbecker et al., 2018).

37 Peak metamorphism of lower to upper greenschist-facies conditions occurred between 17 and 22 Ma  
38 in all external crystalline massifs (Mont Blanc, Aar massifs and the Gotthard nappe, Challandes et al.,  
39 2008; Rolland et al., 2008; Cenko-Tok et al., 2014; Nibourel et al., 2018). Their subsequent  
40 exhumation has been investigated using thermochronology by a number of studies (e.g. Schaer et al.  
41 1975, Wagner et al. 1977; Michalski and Soom, 1990; Vernon et al., 2009; Glotzbach et al., 2010).  
42 While some studies concluded that exhumation was episodic (Vernon et al. 2009), others suggest  
43 relatively constant exhumation rates of 0.5-0.7 km/My since 14 My (Michalski and Soom, 1990;  
44 Glotzbach et al., 2010). The timing of the first surficial exposure of the external massifs has, however,  
45 never been constrained, because estimates of their total thickness have not yet been established. In  
46 most geometric reconstructions (e.g. Pfiffner, 1986, 2017; Schmid et al., 2004), the contact between  
47 the crystalline basement and the overlying Mesozoic cover is assumed to be relatively flat, and the top  
48 of the crystalline basement is hypothesized to be less than one kilometer above the modern  
49 topography. Conversely, a new reconstruction of this tectonic contact allows for a substantially greater  
50 amount (~8 km) of (now eroded) crystalline rock on top of the present-day topography (Nibourel et  
51 al., 2018).

52 This study aims to constrain the timing of exposure, and thus the beginning of sediment supply from  
53 the external crystalline massifs, by determining the provenance of the foreland basin deposits.  
54 Sediments preserved in the northern peripheral foreland basin of the Central Alps, the Swiss part of  
55 the Molasse basin, are a well-studied archive recording tectonic and climatic adjustments in the central  
56 orogen between ca. 32 and 14 My ago (Schlunegger et al., 1993, 1996; Kempf et al., 1999; Spiegel et  
57 al., 2000; Kuhlemann and Kempf, 2002; von Eynatten, 2003; Schlunegger and Kissling, 2015). So far,  
58 the provenance of the Molasse deposits has been investigated using optical heavy mineral analysis,  
59 framework petrography and both bulk and single-grain geochemical techniques, including epidote  
60 geochemistry and cooling ages derived from zircon fission track analysis and Ar/Ar dating of white  
61 mica (Spiegel et al., 2000, 2002; von Eynatten, 2003; von Eynatten and Wijbrans, 2003). Conclusive  
62 evidence for a contribution from the external crystalline massifs, however, has remained elusive,  
63 leading to the assumption that their exposure must post-date the youngest preserved (ca. 14 My-old)  
64 Molasse sediments (von Eynatten, 2003).

65 In this study, we use detrital garnet major element geochemistry in Miocene deposits preserved in the  
66 central part of the Swiss foreland basin. The great compositional variability displayed by garnet from  
67 different source rocks means that it is a useful provenance tracer in a variety of settings (Spear, 1994;  
68 Mange and Morton, 2007). Furthermore, it is a common heavy mineral in (orogenic) sediments  
69 (Garzanti and Andò, 2007) and is relatively stable during transport and diagenesis (Morton and



70 Hallsworth, 2007). In the Central Alps, detrital garnet has recently been shown to be a valuable  
71 provenance indicator, especially for distinguishing detritus supplied from the external crystalline  
72 massifs (Stutenbecker et al., 2017). We aim (1) to provide additional provenance information to  
73 unravel the Miocene history of the Molasse deposits and its tectonic forcing and (2) to test whether  
74 detritus from the external massifs is present in the younger Molasse deposits in order to give  
75 independent constraints on the timing of crystalline basement exhumation.

### 76 1.1 Geological Setting

77 The Central Alps evolved through convergence between the European continental margin in the north  
78 and the Adriatic plate in the south (Schmid et al., 1996). Convergence started in the late Cretaceous  
79 with the subduction of the alpine Tethys ocean below the Adriatic microplate (Froitzheim et al., 1996),  
80 and ceased in the Paleogene after the European continental lithosphere entered the subduction zone.  
81 These Cretaceous to early Neogene orogenic processes are reflected by the syn-orogenic deposition of  
82 deep-marine flysch units preserved throughout the Alps (see e.g. Wildi, 1985; Winkler 1996). Around  
83 32 Ma ago, the sedimentation style in the northern foreland basin changed from marine, flysch-like  
84 deposition to shallow marine and terrestrial sedimentation. This is thought to represent the transition to  
85 Molasse-type sedimentation in an overfilled basin and is discussed to be potentially related to a  
86 breakoff of the European slab around the time of the Eocene-Oligocene boundary (e.g. Sinclair et al.  
87 1991; Sinclair 1997; Schlunegger and Kissling, 2015). Since this time, the northern foreland basin has  
88 become a major sink of orogenic detritus and an important sedimentary archive.  
89 The sediments in the Swiss part of the northern foreland basin are divided into four litho-stratigraphic  
90 units that represent two shallowing- and coarsening-up megacycles (Schlunegger et al., 1998). The  
91 first cycle consists of the Rupelian Lower Marine Molasse (LMM) and the Chattian and Aquitanian  
92 Lower Freshwater Molasse (LFM). The second megacycle comprises a transgressive facies of  
93 Burdigalian age (the Upper Marine Molasse, UMM) overlain by Langhian to Serravalian deposits of  
94 the Upper Freshwater Molasse (UFM). The depositional ages of these units were constrained using  
95 mammal biostratigraphy and magnetostratigraphy (Engesser, 1990; Schlunegger et al., 1996).  
96 Throughout the Oligocene and the Miocene, the proximal Molasse deposits are thought to have been  
97 formed through a series of large alluvial fans (Fig. 1) aligned along the alpine thrust front  
98 (Schlunegger et al., 1993; Kuhlemann and Kempf, 2002). The more distal parts of the basin were  
99 instead characterized by axial drainage directed towards the Paratethys in the East/Northeast (31-20  
100 My) and the Western Mediterranean Sea in the Southwest (after 20 My), respectively (Kuhlemann and  
101 Kempf, 2002). Whereas the more distal deposits could be significantly influenced by long-distance  
102 transport from the northeast or southwest, the alluvial fans are thought to carry a local provenance  
103 signal from the rocks exposed immediately south of each fan system due to their proximal nature.

104 The hinterland of the central Swiss foreland basin comprises, from north to south, potential source  
105 rocks derived from the following architectural elements (Figs. 1, 2):

- 106 (1) The Prealps Romandes; a stack of non-metamorphic and weakly metamorphosed sedimentary  
107 cover nappes (Mesozoic carbonates and Cretaceous-Eocene flysch), interpreted as the  
108 accretionary wedge of the alpine Tethys, detached from its basement and thrust northwards  
109 onto the European units.
- 110 (2) The Helvetic nappes; the non- or very low-grade metamorphic sedimentary cover sequence of  
111 the European continental margin (mostly Mesozoic carbonates).
- 112 (3) The external crystalline massifs; lentoid-shaped autochthonous bodies of European continental  
113 crust that consist of a pre-Variscan polycyclic gneiss basement intruded by Upper  
114 Carboniferous to Permian granitoid rocks and an overlying metasedimentary cover. They were  
115 buried within the Alpine nappe stack in the Oligocene (Cenki-Tok et al., 2014), reaching



- 116 greenschist facies peak-metamorphic conditions between 17 and 22 My ago (Fig. 2) and were  
117 exhumed during the Miocene. The Gotthard nappe, although not a “massif” *sensu stricto*  
118 because of its allochthonous nature, will be included into the term “external crystalline  
119 massifs” from here on, because the timing and the rates of exhumation are comparable  
120 (Glotzbach et al., 2010).
- 121 (4) The Lepontine dome; an allochthonous nappe stack of European Paleozoic gneiss basement  
122 and its Mesozoic metasedimentary cover (Berger et al. 2005). Amphibolite-facies peak  
123 metamorphism (Frey and Ferreiro Mählmann 1999, Fig. 2) in the Lepontine occurred  
124 diachronously at around 30-27 My ago in the south (Gebauer, 1999) and as late as 19 My ago  
125 in the north (Janots et al., 2009). Although the onset of exhumation of the Lepontine dome  
126 might have been equally diachronous, it is generally assumed to have occurred before 23 My  
127 ago (Hurford, 1986).
- 128 (5) The Penninic nappes, containing ophiolites of the alpine Tethys as well as the continental crust  
129 of Briançonnais, a microcontinent located within the alpine Tethys between the southern  
130 Piedmont-Ligurian ocean and the northern Valais trough (Schmid et al. 2004).
- 131 (6) The Austroalpine nappes, containing the basement and sedimentary cover of the Adriatic plate  
132 with a Cretaceous (“Eoalpine”, ca. 90-110 My) metamorphic peak of greenschist facies  
133 conditions (Schmid et al. 2004). Although the Austroalpine nappes are found exclusively in  
134 the Eastern Alps to the east of the Lepontine dome today, we mention them here as well,  
135 because they were probably part of the nappe stack in the Central Alps prior to their erosion  
136 during the Oligocene and Miocene.
- 137 (7) The Sesia/Dent Blanche nappe, probably representing rifted segments of the basement and  
138 sedimentary cover of a distal part of the Adriatic plate (Froitzheim et al. 1996). In contrast to  
139 the Austroalpine nappes, the Sesia/Dent Blanche nappe was subducted and exposed to  
140 blueschist-facies (Bousquet et al. 2012, Fig. 2) to eclogite-facies metamorphism (e.g.  
141 Oberhänsli et al. 2004).
- 142

## 143 1.2 Compositional trends in the Napf fan

144 Rocks from the Central Alps are generally considered as the major sediment source of all proximal  
145 Molasse basin deposits, while compositional changes in the foreland are thought to directly reflect  
146 tectonic and erosional processes in the immediate alpine hinterland (Matter, 1964; Schlunegger et al.,  
147 1993; 1998). The compositional evolution in the basin is diachronous and not uniform between the  
148 different fan systems (e.g. Schlunegger et al., 1998; Spiegel et al., 2000; von Eynatten, 2003). In this  
149 study, we will focus on the Napf fan, located in the central part of the basin, which is the most likely to  
150 archive a provenance signal related to external massif exhumation due to its proximity to the large  
151 crystalline basement slices of the Aar massif and the Gotthard nappe (Fig. 1). In the Napf fan, three  
152 major compositional trends have been previously identified (Fig. 3):

153 (Phase 1) Between ~31 and ~25 My ago, the heavy minerals are dominated by the zircon-tourmaline-  
154 rutile (ZTR) assemblage and garnet (von Eynatten, 2003). Rock fragments are dominantly of  
155 sedimentary origin and zircon fission track ages are Paleozoic to late Mesozoic (Spiegel et al., 2000).  
156 This phase is consistently interpreted by different authors to reflect the erosion of (Austroalpine)  
157 flysch-like sedimentary cover nappes, which are structurally highest in the central alpine nappe stack  
158 (Schlunegger et al., 1998; Spiegel et al., 2000; von Eynatten, 2003).

159 (Phase 2) 25-21 My ago: Around 25 My ago, the occurrence of epidote as well as an increase in  
160 granitic rock fragments mark a major compositional change in the foreland. The presence of  
161 characteristic colorful granite pebbles suggests an origin from the Austroalpine Bernina nappe (Matter,



162 1964). Sediments of this phase clearly reflect the down-cutting into crystalline basement and are  
163 consistent with a continuation of a normal unroofing sequence. Additionally, (Schlunegger et al.,  
164 1998) report the occurrence of quartzite pebbles, possibly sourced from the Penninic Siviez-Mischabel  
165 nappe and argue that parts of the epidote could originate from Penninic ophiolites as well, thus  
166 suggesting that erosion might have already reached down into the Penninic nappes. Spiegel et al.,  
167 (2002) argued against this Penninic contribution based on the  $^{87}\text{Sr}/^{86}\text{Sr}$  and  $^{143}\text{Nd}/^{144}\text{Nd}$  isotopic  
168 signatures of the epidote.

169 (Phase 3) 21-14 My ago: At ~21 My, metamorphic rock fragments occur in the sediments, while the  
170 heavy mineral assemblages remain epidote-dominated and overall similar to the second phase. Zircon  
171 fission track ages are exclusively Cenozoic (ages peaks between ~32 and ~19 Ma). In contrast to the  
172 first two phases, the sediment composition allows several, partially contradicting interpretations.  
173 Whilst petrographical and mineralogical data might suggest recycling and sediment mixing (von  
174 Eynatten, 2003), young  $^{40}\text{Ar}/^{39}\text{Ar}$  cooling ages in white mica (von Eynatten, 2003; von Eynatten and  
175 Wijbrans, 2003) and exclusively young zircon fission track ages (Spiegel et al., 2000) point to an  
176 additional, newly exhumed source that these authors identify as the Lepontine dome. Based on the  
177 abundance of flysch pebbles after ~21 My, Schlunegger et al. (1998) favor an alternative scenario, in  
178 which the erosional front shifted northwards into the flysch nappes of the Prealps Romandes.  
179 Furthermore, the isotopic signature of detrital epidotes suggests a contribution of mantle source rocks  
180 between ca. 21 and 19 My ago, which could point to a contribution by Penninic ophiolites (Spiegel et  
181 al., 2002). However, this is not reflected in the heavy mineral spectra (von Eynatten, 2003), which do  
182 not contain typical ophiolite minerals such as Cr-spinel.

183 In none of these scenarios were the external crystalline massifs considered as a possible sediment  
184 source. The exact time of their surficial exposure is unknown, but it is believed to post-date the  
185 youngest preserved Molasse sediments. This interpretation is based on the lack of granitic pebbles  
186 attributable to the external massifs in the Molasse (Trümpy, 1980) and on structural reconstructions  
187 (e.g. Pfiffner, 1986) in combination with thermochronological data (e.g. Michalski and Soom, 1990).

## 188 2. Sampling strategy and methodology

189 In order to characterize the detrital garnets in the foreland, three samples were taken from 25 My-, 19  
190 My- and 14 My-old fine- to medium-grained fluvial sandstones within the Napf fan deposits located  
191 ca. 40 kilometers to the East and Southeast of Bern in the central part of the Swiss Molasse basin. The  
192 exact sampling sites were chosen based on the availability of published petrographical, chemical and  
193 mineralogical data (von Eynatten, 2003) as well as magnetostratigraphic calibration (Schlunegger et  
194 al., 1996).

195 Because the potential source rocks were already narrowed down to particular regions based on other  
196 provenance proxies, and because many of these rocks are still preserved in the alpine chain today, it is  
197 possible to compare potential source compositions to the detrital ones. For comparison we used  
198 detrital data from Stutenbecker et al. (2017) as well as published source rock data from different units  
199 across the Central Alps (Steck and Burri, 1971; Chinner and Dixon, 1973; Ernst and Dal Piaz, 1978;  
200 Hunziker and Zingg, 1980; Oberhänsli, 1980; Sartori, 1990; Thélin et al., 1990; Reinecke, 1998; von  
201 Raumer et al., 1999; Cartwright and Barnicoat, 2002; Bucher and Bousquet, 2007; Angiboust et al.,  
202 2009; Bucher and Grapes, 2009; Weber and Bucher, 2015).

203 In addition, three river sand samples were collected from small monolithological catchments (3-30  
204 km<sup>2</sup>) draining garnet-bearing potential source rocks that were previously not, or only partially,  
205 considered in the literature. We prefer this “tributary sampling approach” (see e.g. Stutenbecker et al.,  
206 2017) over sampling specific source rocks, because small monolithological catchments are more likely



207 to comprise all garnet varieties of the targeted source rock and to average out differences in garnet  
208 fertility. The targeted source areas are located within the Gurnigel flysch (Prealpes Romandes), the  
209 Antigorio nappe orthogneisses of the Lepontine dome, and the Lebendun nappe paragneisses of the  
210 Lepontine dome (Fig.1). Sample characteristics are summarized in Table 1 and Table 2. For detailed  
211 lithological descriptions of the sampled sites in the Napf area, see Schlunegger et al. (1993) and von  
212 Eynatten (2003).

213 The sandstone samples were carefully disintegrated using a jaw breaker and a pestle and mortar. The  
214 disintegrated sandstones as well as the source rock tributary sands were sieved into four grain size  
215 classes of <63  $\mu\text{m}$ , 63-125  $\mu\text{m}$ , 125-250  $\mu\text{m}$  and >250  $\mu\text{m}$ . The fractions of 63-125  $\mu\text{m}$  and 125-250  
216  $\mu\text{m}$  were further processed in sodium polytungstate heavy liquid at 2.85  $\text{g}/\text{cm}^3$  to concentrate heavy  
217 minerals. The heavy mineral concentrates were dried and, depending on the obtained amounts, split  
218 into 2-4 parts using a microsplitter. All measured garnet grains were hand-picked from the concentrate  
219 of one split part per fraction under a binocular microscope.

220 The grains were subsequently arranged in lines on sticky tape, embedded into epoxy resin, ground  
221 with SiC abrasive paper (grits 400, 800, 1200, 2500, 4000), polished using 3, 1 and  $\frac{1}{4}$   $\mu\text{m}$  diamond  
222 suspensions and graphite-coated. Major element oxides were analyzed using a JEOL JXA-8200  
223 electron probe micro-analyzer at the Institute of Geological Science at University of Bern,  
224 Switzerland, under standard operating conditions for garnet (see Giuntoli et al., 2018): accelerating  
225 voltage of 15 KeV, electron beam current of 15 nA, beam diameter of 1 $\mu\text{m}$ , 20 s peak acquisition time  
226 for Si, Ti, Al, Fe, Mn, Mg, Ca and 10 s for both backgrounds. Natural and synthetic standard olivine  
227 ( $\text{SiO}_2$ , MgO, FeO), anorthite ( $\text{Al}_2\text{O}_3$ , CaO) ilmenite ( $\text{TiO}_2$ ) and tephroite (MnO) were used for  
228 calibration by applying a CITIZAF correction (Armstrong, 1984). Garnet compositions were measured  
229 as close as possible to the geometric centers of grains, unless the area was heavily fractured. In some  
230 randomly selected grains core and rim compositions were measured to identify intra-grain chemical  
231 variability; these core/rim pairs are reported separately in Stutenbecker (2019).

232 Molecular proportions were calculated from the measured main oxide compositions on the base of 12  
233 anhydrous oxygens. Because ferric and ferrous iron were not measured separately ( $\text{FeO} = \text{Fe}_{\text{total}}$ ), the  
234  $\text{Fe}^{2+}/\text{Fe}^{3+}$  ratio was determined based on charge balance (Locock, 2008). Garnet endmember  
235 compositions were subsequently calculated using the Excel spreadsheet by Locock (2008). Garnet is a  
236 solid solution between different endmembers, the most common ones being almandine ( $\text{Fe}_3\text{Al}_2\text{Si}_3\text{O}_{12}$ ),  
237 grossular ( $\text{Ca}_3\text{Al}_2\text{Si}_3\text{O}_{12}$ ), pyrope ( $\text{Mg}_3\text{Al}_2\text{Si}_3\text{O}_{12}$ ), spessartine ( $\text{Mn}_3\text{Al}_2\text{Si}_3\text{O}_{12}$ ) and andradite  
238 ( $\text{Ca}_3\text{Fe}_2\text{Si}_3\text{O}_{12}$ ). The relative proportions of these endmember components depend on bulk rock  
239 composition and intensive parameters (such as temperature and pressure) which can vary substantially  
240 depending on the metamorphic or magmatic history of the protolith (Deer et al., 1992; Spear, 1994).  
241 The data were plotted and classified using the ternary diagram of Mange and Morton (2007) as well as  
242 the linear discriminant function method of Tolosana-Delgado et al. (2018) based on a global data  
243 compilation on garnet compositions from different source rocks (Krippner et al., 2014).

### 244 3. Results

245 Most of the detrital garnets are dominated by the Fe-rich almandine endmember with varying amounts  
246 of grossular, pyrope, spessartine and andradite (Fig. 4). Other endmembers (e.g. uvarovite) are  
247 negligible. Minimum, maximum and average endmember contents are summarized in Table 3; for the  
248 full dataset we refer to Stutenbecker (2019). Garnet compositions do not differ significantly between  
249 the two analyzed grain size fractions of the same sample, although some slight variations are visible in  
250 the ternary plot (Fig. 4): In sample LS2016-18 (25 My, Fig. 4a) garnets of the 125-250  $\mu\text{m}$  fraction  
251 tend to be enriched in pyrope with respect to garnets of the 63-125  $\mu\text{m}$  fraction. In sample LS2018-5



252 (19 My, Fig. 4b) 4 “outliers” that are very pyrope- and grossular-rich (n=2) or grossular- and  
253 andradite-rich (n=2) occur only in the 63-125  $\mu\text{m}$  grain size fraction. Furthermore, garnet grains of the  
254 63-125  $\mu\text{m}$  fraction are more frequently grossular-rich compared to the 125-250  $\mu\text{m}$  fraction. In  
255 sample LS2017-3 (14 My, Fig. 4c), the 63-125  $\mu\text{m}$  fraction contains some garnet grains (n=8) of high  
256 almandine and low grossular content that are absent in the 125-250  $\mu\text{m}$  fraction.

257  
258

259 Although some individual garnets show distinct internal compositional zoning from core to rim, the  
260 intra-grain chemical variability is generally negligible (see Stutenbecker, 2019).

261 According to the ternary classification plot of Mange and Morton (2007), the major part of garnet in  
262 all three samples (>80 %) belong to the B-type and thus point to a dominant amphibolite-facies source  
263 rock (Table 4). Minor portions are derived from C-type (high-grade metabasic), A-type (granulite  
264 facies) and D-type (metasomatic) sources. Classification through linear discriminant analysis  
265 (Tolosana-Delgado et al., 2018) yields a similar trend with generally high proportions of amphibolite-  
266 facies source rocks (class B-garnets, >70 %, Table 4). Some grains (5 %, 3 % and 12 % in the 25 My-,  
267 19 My- and 14 My-old samples, respectively) were classified as igneous garnet (Table 4).

268 Distinct compositional changes between the 25 My-, 19 My- and 14 My-old Molasse sediments are  
269 mostly related to the ratio of almandine and grossular contents (Table 3, Fig. 5). At 25 My, garnets are  
270 dominantly almandine-rich (average 70 %) and grossular-poor (average 9 %). At 19 My, both  
271 grossular-poor and grossular-richer garnets occur (average 16 %). Garnets in the 14 My-old sample are  
272 generally almandine-poorer (average 50 %) and grossular-rich (average 32 %). This implies (1) that  
273 garnets contained in the younger sediment (14 and, to some extent, 19 My) were not recycled in  
274 significant amounts from the older Molasse strata and (2) that at least two sources supplied B-type  
275 garnets during Molasse deposition.

276

277 Garnet compositions from the three potential source rock samples analyzed in this study are shown in  
278 Fig. 4d (Leptontine paragneiss and Leptontine orthogneiss) and Fig. 4e (Gurnigel flysch). The average  
279 compositions are displayed in Fig. 6; for the full dataset we refer to Stutenbecker (2019). Likewise,  
280 average compositions of garnet from the literature (external massif granite garnets, eclogite facies  
281 garnets and granulite facies garnets) are displayed in Fig. 6.

282

283 All source rocks, except for the external crystalline massif granites, supply almandine-dominated (i.e.  
284 >50 % almandine-component) garnet. The andradite content in all source rock garnets is very low, but  
285 they contain varying amounts of grossular, spessartine and pyrope. Garnets from the Leptontine  
286 gneisses (Fig. 4d) are generally almandine-rich, but those in the paragneiss tend to be grossular-richer  
287 (22 %) compared to the ones in the orthogneiss (11 %). The Gurnigel flysch garnets (Fig. 4e) are  
288 almandine-rich with elevated pyrope contents (14 %). Garnets from the external crystalline massifs  
289 (Fig. 4f) are unusually rich in grossular (35 %) and spessartine (21 %), and the almandine content is  
290 much lower than in the other source rock garnets (34 %). Eclogite-facies garnets have high grossular  
291 (23 %) and pyrope (16 %) contents (Fig. 4g). Granulite-facies garnets (Fig. 4g) have on average the  
292 highest pyrope content of all source rock garnets (25 %).

## 293 4. Discussion

### 294 4.1 Origin of amphibolite-facies garnets

295 According to the compositional classification of Mange and Morton (2007) and Tolosana-Delgado et  
296 al. (2018), the majority of detrital garnet grains in the Molasse were derived from amphibolite-facies



297 source rocks (“B-type”). In the Central Alps, amphibolite-facies conditions of alpine age were only  
298 reached in the Lepontine nappes (Fig. 2). However, many gneisses in the area preserve a pre-Mesozoic  
299 amphibolite-facies metamorphic signature as well (Frey et al., 1999), for example in the Austroalpine  
300 Bernina nappe (Spillmann, 1993; Spillmann and Büchi, 1993), the middle Penninic Briançonnais  
301 basement (Sartori et al., 2006) or the polycyclic basement of the external massifs (von Raumer et al.,  
302 1999). In fact, the Gurnigel flysch, a Late Cretaceous to Eocene flysch nappe in the Prealps Romandes  
303 that did not undergo alpine metamorphism (Fig. 2), contains almost exclusively almandine-rich B-type  
304 garnets (Fig. 4e).  
305 These considerations indicate that, following the classification scheme of Mange and Morton (2007)  
306 alone, the provenance of Alpine B-type garnets remains ambiguous. However, petrographic findings  
307 as well as zircon fission-track analysis and Ar/Ar dating in white mica (Spiegel et al., 2000; von  
308 Eynatten, 2003; von Eynatten and Wijbrans, 2003) strongly suggest a compositional change ca. 21 My  
309 ago towards a metasedimentary source with a young cooling history. These authors relate this shift to  
310 the erosion of the sedimentary cover of the Lepontine dome. Source rock samples taken within the  
311 Lepontine dome from the crystalline basement (Antigorio nappe orthogneiss) and the meta-  
312 sedimentary cover (Lebendun nappe paragneiss) contain generally almandine-rich garnets, but those  
313 from the paragneiss tend to be richer in grossular than those from the orthogneisses (Fig. 4). Because  
314 the amount of grossular-rich garnet is higher in the 19 My-old sample compared to the 25 My-old  
315 sample, the data could support an origin from the Lepontine meta-sedimentary cover.

#### 316 4.2 Origin of granulite-facies garnets

317 Granulite-facies garnet grains with relatively high pyrope and low grossular contents (“A-type” and  
318 “Class C” garnets according to Mange and Morton (2007) and Tolosana-Delgado et al. (2018),  
319 respectively) are only frequent in the 19 My-old Molasse sample (ca. 8-9 %, Table 3). Alpine  
320 Granulite-facies metamorphic conditions in the Central Alps were only reached in the Gruf complex  
321 located close to the Insubric line between the Lepontine dome and the Bergell intrusion (Fig. 2).  
322 Furthermore, there is evidence for pre-Mesozoic granulite-facies metamorphism in some rocks in the  
323 Ivrea zone south of the Insubric line (Hunziker and Zingg, 1980), in the Sesia Zone (Engi et al., 2018;  
324 Giuntoli et al., 2018) and in the Dent Blanche nappe (Angiboust et al., 2009). It is unlikely that erosion  
325 reached so far to the South during the Miocene, because the Penninic and probably also the exhuming  
326 Lepontine nappe stack would have acted as a topographic barrier to the fluvial drainage network.  
327 However, it was proposed that the flysch sediments preserved in the Prealps Romandes were partially  
328 fed by these units during the Late Cretaceous and the Eocene (Wildi, 1985; Ragusa et al., 2017). This  
329 interpretation is supported by the Gurnigel flysch sample (Fig. 4e), which contains garnet of granulite-  
330 facies type. A recycled flysch origin is supported further by the abundance of flysch sandstone pebbles  
331 in Molasse strata of the same age (Schlunegger et al., 1998).

#### 332 4.3 Origin of eclogite-facies garnets

333 The 19 My-old sample contains two grains with very high pyrope contents classified as eclogite-facies  
334 garnets (“Ci-type” and “Class A” garnets according to Mange and Morton (2007) and Tolosana-  
335 Delgado et al. (2018), respectively). In the 14 My-old sample, 15 % of grains were classified as  
336 eclogite-facies garnets as well following the Mange and Morton (2007) approach, although these  
337 grains are pyrope-poorer compared to the garnets in the 19 My-old sample and therefore probably  
338 originate from a different source. Eclogite-facies garnets are known from metamorphic rocks of the  
339 upper Penninic alpine ophiolites (e.g. Bucher and Grapes, 2009; Weber and Bucher, 2015, Fig. 2), but  
340 also from Paleozoic (?) gneisses of the middle Penninic Briançonnais basement (Sartori, 1990; Thélin  
341 et al., 1990). In addition, the Gurnigel flysch contains a minor, pyrope-rich population of garnets (Fig.  
342 4e). Detrital garnet compositions similar to the ones in the 14 My-old sample were reported from the  
343 Goneri river draining the Gotthard nappe (Stutenbecker et al., 2017).





344 Overall the eclogitic component in all three samples is only minor, thus supporting results from von  
345 Eynatten (2003), who concluded that eclogites were not a major source during the Miocene in the  
346 Napf area.

#### 347 4.4 Origin of “igneous” garnets

348 Of the garnets from the youngest, 14 My-old Molasse sample, 12 % can be classified as igneous  
349 (“Class E”, Table 4) according to Tolosana-Delgado et al. (2018). Their high grossular and very low  
350 pyrope content distinguishes them clearly from all the other, generally more almandine-rich, garnets.  
351 In the classification scheme after Mange and Morton (2007), however, this type of garnet plots in the  
352 D-type or in the rightmost part of the B-type or field (Fig. 4, Table 4). The detrital garnet signature of  
353 the 14 My-old sample mirrors almost exactly the compositional range of garnets from the external  
354 crystalline massifs (Fig. 4c, 4f). In the external crystalline massifs, these garnets grew in Permo-  
355 Carboniferous plutons under alpine greenschist-facies metamorphic conditions (Steck and Burri, 1971,  
356 Fig. 2). They are restricted to the granitoid basement of the external massifs and do not occur  
357 anywhere else in the Central Alps, which makes them an excellent provenance proxy (Stutenbecker et  
358 al., 2017). A further distinction among garnets supplied by the different plutons (e.g. the Central Aar  
359 granite from the Aar massif, the Rotondo granite from the Gotthard nappe or the Mont Blanc granite  
360 from the Mont Blanc massif) is not possible based on garnet major element geochemistry alone  
361 (Stutenbecker et al., 2017).

#### 362 4.5 Implications for the evolution of the Alpine orogen

363 Previous provenance studies have identified meta-sedimentary detritus in the youngest (ca. 14 My old)  
364 Molasse and located its source in the unroofing sedimentary cover of the Lepontine dome (von  
365 Eynatten, 2003). This was strongly supported by the very young zircon fission-track ages that match  
366 the exhumation pattern of the Lepontine dome. However, garnet compositions in the youngest  
367 Molasse sandstones are not comparable to Lepontine garnets sampled in this study nor to any detrital  
368 garnet found in the main rivers draining the Lepontine dome today (Andò et al., 2014).  
369 Instead, the occurrence of grossular- and spessartine-rich garnets in the 14 My-old Molasse mark a  
370 distinct provenance change compared to the 19 My-old deposits that was not noticed in previous  
371 studies (Schlunegger et al., 1998; Spiegel et al., 2000; von Eynatten, 2003). Garnets of this particular  
372 composition are described from the Permo-Carboniferous plutons intruded into the crystalline  
373 basement of the Aar and Mont Blanc massifs and the Gotthard nappe (Steck and Burri, 1971). Such  
374 particular chemical composition provides a unique sedimentary fingerprint (Stutenbecker et al., 2017).  
375 Their occurrence in the youngest Molasse sediments has important implications for the tectonic  
376 evolution of the orogen. Until now, the surficial exposure of the external massifs in the Central Alps  
377 was thought to post-date Molasse deposition. This interpretation relies principally on the absence of  
378 pebbles of external massif origin (e.g. Aare granite) in the foreland basin (Trümpy, 1980). However,  
379 many alpine granites closely resemble each other, especially if present as altered pebbles in the  
380 Molasse deposits, and hence it is difficult to discount a specific source only on this basis. Further  
381 support of late surficial exposure of the external massifs comes from structural reconstructions (e.g.  
382 Pfiffner, 1986; 2017), that have located the top of the crystalline basement similar to the modern  
383 topography, based on a relatively flat-lying contact between the crystalline basement and the overlying  
384 Mesozoic sedimentary cover (Fig. 7a). According to this model and the published exhumation rates of  
385 0.5-0.7 km/My (Michalski and Soom, 1990; Glotzbach et al., 2010), the top of the basement must have  
386 been buried 7-10 km below the surface 14 Ma ago. However, Nibourel et al. (2018) have recently  
387 proposed a revised geometry of the contact between crystalline basement and overlying cover, which  
388 allows ca. 8 km of additional crystalline basement on top of the present-day topography (Fig. 7b). The  
389 presence of external massif-sourced garnets in the youngest Molasse deposits provides independent  
390 evidence that parts of the crystalline crust comprised in the external massifs were already at the



391 surface at ca. 14 Ma. Assuming the aforementioned average exhumation rates, 7-10 km of crystalline  
392 basement would have already been exhumed (and subsequently eroded) during the past 14 My, which  
393 is in good agreement with the geometric reconstructions by Nibourel et al. (2018).

#### 394 5. Conclusions

395 Garnet geochemistry is a useful tool to further constrain the provenance of sediments in orogens such  
396 as the Central Alps. We have demonstrated that it is possible to distinguish detrital garnets using a  
397 combination of garnet classification schemes (Mange and Morton, 2007; Tolosana-Delgado et al.,  
398 2018) and case-specific comparison with available alpine source rock compositions (Stutenbecker et  
399 al., 2017). For the Miocene deposits of the Swiss Molasse basin we were able to (1) confirm the  
400 provenance shift possibly related to the exhumation of the Lepontine dome between 25 and 19 My ago  
401 as suggested by previous studies (von Eynatten, 2003) and (2) to identify an additional provenance  
402 shift between ca. 19 and 14 My ago that had not been noticed before. The latter shift before 14 My ago  
403 is related to the erosion of granites from the external crystalline massifs, which provides a minimum  
404 age for their surficial exposure and corroborates their recently revised structural geometry (Fig. 7b).

#### 405 Author contribution

406 LS designed the project. AM helped during field work and sample collection. PT and PL gave advice  
407 for sample preparation, supported the microprobe measurements and data acquisition at the University  
408 of Bern. LS prepared the manuscript with contributions by all co-authors.

#### 409 Acknowledgements

410 This project was financially supported by a post-doctoral research grant awarded to L. Stutenbecker by  
411 the International Association of Sedimentologists (IAS). We would like to thank Fritz Schlunegger for  
412 guidance in the field and Alfons Berger and Lukas Nibourel for stimulating discussions.

#### 413 References

- 414 Andò, S., Morton, A.C., and Garzanti, E.: Metamorphic grade of source rocks revealed by chemical  
415 fingerprints of detrital amphibole and garnet. *Geol. Soc. Spec. Publ.*, 386, 351–371,  
416 doi:10.1144/SP386.5, 2014.
- 417 Angiboust, S., Agard, P., Jolivet, L., and Beyssac, O.: The Zermatt-Saas ophiolite: The largest (60-km  
418 wide) and deepest (c. 70-80km) continuous slice of oceanic lithosphere detached from a subduction  
419 zone? *Terra Nova*, 21, 171–180, doi:10.1111/j.1365-3121.2009.00870.x, 2009.
- 420 Armstrong, J.T.: Quantitative analysis of silicate and oxide minerals: a reevaluation of ZAF  
421 corrections and proposal for new Bence–Albee coefficients, in: *Microbeam Analysis*, edited by Romig,  
422 A.D. and Goldstein, J.I., San Francisco Press, USA, 208–212, 1984.
- 423 Baran, R., Friedrich, A.M., and Schlunegger, F.: The late Miocene to Holocene erosion pattern of the  
424 Alpine foreland basin reflects Eurasian slab unloading beneath the western Alps rather than global  
425 climate change. *Lithosphere*, 6, 124–131, doi:10.1130/L307.1, 2014.
- 426 Berger, A., Mercolli, I., and Engi, M.: The central Lepontine Alps: Notes accompanying the tectonic  
427 and petrographic map sheet Sopra Ceneri (1:100'000). *Schweiz. Miner. Petrog.*, 85, 109–146, 2005.
- 428 Bousquet, R., Oberhänsli, R., Schmid, S.M., Berger, A., Wiederkehr, M., Robert, C., Möller, A.,  
429 Rosenberg, C., Zeilinger, G., Molli, G., and Koller, F.: *Metamorphic Framework of the Alps*.  
430 Commission for the geological map of the world, Paris, 2012.



- 431  
432 Bucher, S., and Bousquet, R.: Metamorphic evolution of the Briançonnais units along the ECORS-  
433 CROP profile (Western Alps): New data on metasedimentary rocks. *Swiss J. Geosci.*, 100, 227–242,  
434 doi:10.1007/s00015-007-1222-4, 2007.
- 435 Bucher, K., and Grapes, R.: The eclogite-facies Allalin gabbro of the Zermatt-Saas ophiolite, Western  
436 alps: A record of subduction zone hydration. *J. Petrol.*, 50, 1405–1442, doi:10.1093/petrology/egp035,  
437 2009.
- 438 Cartwright, I., and Barnicoat, A.C.: Petrology, geochronology, and tectonics of shear zones in the  
439 Zermatt-Saas and Combin zones of the Western Alps. *J. Metamorph. Geol.*, 20, 263–281, 2002.
- 440 Cenko-Tok, B., Darling, J.R., Rolland, Y., Dhuime, B., and Storey, C.D.: Direct dating of mid-crustal  
441 shear zones with synkinematic allanite: New in situ U-Th-Pb geochronological approaches applied to  
442 the Mont Blanc massif. *Terra Nova*, 26, 29–37, doi:10.1111/ter.12066, 2014.
- 443 Challandes, N., Marquer, D., and Villa, I.M.: P-T-t modelling, fluid circulation, and <sup>39</sup>Ar-<sup>40</sup>Ar and  
444 Rb-Sr mica ages in the Aar Massif shear zones (Swiss Alps). *Swiss J. Geosci.*, 101, 269–288,  
445 doi:10.1007/s00015-008-1260-6, 2008.
- 446 Chinner, G.A., and Dixon, J.E.: Some high-pressure parageneses of the allalin gabbro, Valais,  
447 Switzerland. *J. Petrol.*, 14, 185–202, doi:10.1093/petrology/14.2.185, 1973.
- 448 Deer, W., Howie, R.A., and Zussmann, J.: An introduction to the rock-forming minerals. New Jersey:  
449 Prentice Hall, 1992.
- 450 Engesser, B.: Die Eomyidae (Rodentia, Mammalia) der Molasse der Schweiz und Savoyens.  
451 Systematik und Biostratigraphie. Schweizer Paläontologische Abhandlungen (112), Basel: Birkhäuser  
452 Verlag, 1990.
- 453 Engi, M., Giuntoli, F., Lanari, P., Burn, M., Kunz, B., and Bouvier, A.S.: Pervasive Eclogitization Due  
454 to Brittle Deformation and Rehydration of Subducted Basement: Effects on Continental Recycling?  
455 *Geochem. Geophys. Geosy.*, 19, 865–881, doi:10.1002/2017GC007215, 2018.
- 456 Ernst, W.G., and Dal Piaz, G. V.: Mineral parageneses of eclogitic rocks and related mafic schists of  
457 the Piemonte ophiolite nappe, Breuil-St Jacques area, Italian Western Alps. *Amer. Mineral.*, 63, 621–  
458 640, 1978.
- 459 von Eynatten, H.: Petrography and chemistry of sandstones from the Swiss Molasse Basin: An archive  
460 of the Oligocene to Miocene evolution of the Central Alps. *Sedimentology*, 50, 703–724,  
461 doi:10.1046/j.1365-3091.2003.00571.x, 2003.
- 462 von Eynatten, H., and Wijbrans, J.R.: Precise tracing of exhumation and provenance using <sup>40</sup>Ar/<sup>39</sup>Ar  
463 geochronology of detrital white mica: the example of the Central Alps. *Geol. Soc. Spec. Publ.*, 208,  
464 289–305, 2003.
- 465 Fox, M., Herman, F., Kissling, E., and Willett, S.D.: Rapid exhumation in the Western Alps driven by  
466 slab detachment and glacial erosion. *Geology*, 43, 379–382, doi:10.1130/G36411.1, 2015.
- 467 Frey, M., Desmons, J., and Neubauer, F.: The new metamorphic map of the Alps: introduction.  
468 *Schweiz. Miner. Petrog.*, 79, 1–4, doi:10.5169/seals-60194, 1999.
- 469 Frey, M., and Ferreiro Mählmann, R.: Alpine metamorphism of the Central Alps. *Schweiz. Miner.  
470 Petrog.*, 79, 135–154, 1999.
- 471 Froitzheim, N., Schmid, S.M., and Frey, M.: Mesozoic paleogeography and the timing of  
472 eclogitefacies in the Alps: A working hypothesis. *Eclogae Geol. Helv.*, 110, 81–110, 1996.
- 473 Garzanti, E., and Andò, S.: Plate Tectonics and Heavy Mineral Suites of Modern Sands.



- 474 Developments in Sedimentology, 58, 741–763, doi:10.1016/S0070-4571(07)58029-5, 2007.
- 475 Gebauer, D.: Alpine geochronology of the Central and Western Alps: new constraints for a complex  
476 geodynamic evolution. Schweiz. Miner. Petrog., 79, 191–208, doi:10.5169/seals-60205, 1999.
- 477 Giuntoli, F., Lanari, P., and Engi, M.: Deeply subducted continental fragments - Part 1: Fracturing,  
478 dissolution-precipitation, and diffusion processes recorded by garnet textures of the central Sesia Zone  
479 (western Italian Alps). Solid Earth, 9, 167–189, doi:10.5194/se-9-167-2018, 2018.
- 480 Glotzbach, C., Reinecker, J., Danišik, M., Rahn, M., Frisch, W., and Spiegel, C.: Thermal history of  
481 the central Gotthard and Aar massifs, European Alps: Evidence for steady state, long-term  
482 exhumation: J. Geophys. Res. - Earth, 115, doi:10.1029/2009JF001304, 2010.
- 483 Handy, M.R., M. Schmid, S., Bousquet, R., Kissling, E., and Bernoulli, D.: Reconciling plate-tectonic  
484 reconstructions of Alpine Tethys with the geological-geophysical record of spreading and subduction  
485 in the Alps. Earth-Sci. Rev., 102, 121–158, doi:10.1016/j.earscirev.2010.06.002, 2010.
- 486 Herwegh, M., Berger, A., Baumberger, R., Wehrens, P., and Kissling, E.: Large-Scale Crustal-Block-  
487 Extrusion During Late Alpine Collision. Sci. Rep., 7, 413, doi:10.1038/s41598-017-00440-0, 2017.
- 488 Hunziker, J.C., and Zingg, A.: Lower palaeozoic amphibolite to granulite facies metamorphism in the  
489 Ivrea zone (Southern Alps, Northern Italy). Schweiz. Miner. Petrog., 60, 181–213, 1980.
- 490 Hurford, A.J.: Cooling and uplift patterns in the Lepontine Alps South Central Switzerland and an age  
491 of vertical movement on the Insubric fault line. Contrib. Mineral. Petr., 92, 413–427,  
492 doi:10.1007/BF00374424, 1986.
- 493 Janots, E., Engi, M., Rubatto, D., Berger, A., Gregory, C., and Rahn, M.: Metamorphic rates in  
494 collisional orogeny from in situ allanite and monazite dating. Geology, 37, 11–14,  
495 doi:10.1130/G25192A.1, 2009.
- 496 Kempf, O., Matter, A., Burbank, D.W., and Mange, M.: Depositional and structural evolution of a  
497 foreland basin margin in a magnetostratigraphic framework: The eastern Swiss Molasse Basin. Int. J.  
498 Earth Sci., 88, 253–275, doi:10.1007/s005310050263, 1999.
- 499 Krippner, A., Meinhold, G., Morton, A.C., and von Eynatten, H.: Evaluation of garnet discrimination  
500 diagrams using geochemical data of garnets derived from various host rocks. Sedimentary Geol., 306,  
501 36–52, doi:10.1016/j.sedgeo.2014.03.004, 2014.
- 502 Kuhlemann, J., and Kempf, O.: Post-Eocene evolution of the North Alpine Foreland Basin and its  
503 response to Alpine tectonics. Sedimentary Geol., 152, 45–78, doi:10.1016/S0037-0738(01)00285-8,  
504 2002.
- 505 Kühni, A., and Pfiffner, O.A.: The relief of the Swiss Alps and adjacent areas and its relation to  
506 lithology and structure: Topographic analysis from a 250-m DEM. Geomorphology, 41, 285–307,  
507 doi:10.1016/S0169-555X(01)00060-5, 2000.
- 508 Locock, A.J.: An Excel spreadsheet to recast analyses of garnet into end-member components, and a  
509 synopsis of the crystal chemistry of natural silicate garnets. Comput. Geosci., 34, 1769–1780,  
510 doi:10.1016/j.cageo.2007.12.013, 2008.
- 511 Mange, M.A., and Morton, A.C.: Geochemistry of heavy minerals. Developments in Sedimentology,  
512 58, 345–391, 2007.
- 513 Matter, A.: Sedimentologische Untersuchungen im östlichen Napfgebiet (Entlebuch - Tal der Grossen  
514 Fontanne, Kt. Luzern). Eclogae Geol. Helv., 57, 315–428, 1964.
- 515 Michalski, I., and Soom, M.: The Alpine thermo-tectonic evolution of the Aar and Gotthard massifs,  
516 Central Switzerland - Fission Track ages on zircon and apatite and K-Ar mica ages. Schweiz. Miner.



- 517 Petrog., 70, 373–387, doi:10.5169/seals-53628, 1990.
- 518 Morton, A.C., and Hallsworth, C.: Stability of Detrital Heavy Minerals During Burial Diagenesis.  
519 Developments in Sedimentology, 58, 215–245, doi:10.1016/S0070-4571(07)58007-6, 2007.
- 520 Nibourel, L., Berger, A., Egli, D., Luensdorf, N.K., and Herwegh, M.: Large vertical displacements of  
521 a crystalline massif recorded by Raman thermometry. *Geology*, 46, 879–882, doi:10.1130/G45121.1,  
522 2018.
- 523 Oberhänsli, R.: P-T Bestimmungen anhand von Mineralanalysen in Eklogiten und Glaukophaniten der  
524 Ophiolite von Zermatt. *Schweiz. Miner. Petrog.*, 60, 215–235, doi:10.5169/seals-46668, 1980.
- 525 Oberhänsli, R., Bousquet, R., Engi, M., Goffé, B., Gosso, G., Handy, M.R., Höck, V., Koller,  
526 F., Lardeaux, J.M., Polino, R., Rossi, P.L., Schuster, R., Schwartz, S., Spalla, I.: *Metamorphic  
527 Structure of the Alps*. CCGM Commission of the Geological Maps of the World, 2004.
- 528 Pfiffner, O.A.: Evolution of the north Alpine foreland basin in the Central Alps, in: *Foreland basins*,  
529 edited by Allen, P.A. and Homewood, P., *Int. As. Sed.*, 8, 219–228, 1986.
- 530 Pfiffner, O.A.: Thick-Skinned and Thin-Skinned Tectonics: A Global Perspective. *Geosciences*, 7, 71,  
531 doi:10.3390/geosciences7030071, 2017.
- 532 Pfiffner, O.A., Schlunegger, F., and Buitter, S.J.H.: The Swiss Alps and their peripheral foreland basin:  
533 Stratigraphic response to deep crustal processes. *Tectonics*, 21, 3.1-3.16, doi:10.1029/2000TC900039,  
534 2002.
- 535 Ragusa, J., Kindler, P., Šegvić, B., and Ospina-Ostios, L.M.: Provenance analysis of the Voiron  
536 Flysch (Gurnigel nappe, Haute-Savoie, France): stratigraphic and palaeogeographic implications:  
537 Springer Berlin Heidelberg, 106, 2619-2651, doi:10.1007/s00531-017-1474-9, 2017.
- 538 von Raumer, J.F., Abrecht, J., Bussy, F., Lombardo, B., Menot, R.-P., and Schaltegger, U.: The  
539 Palaeozoic metamorphic evolution of the Alpine External Massifs. *Schweiz. Miner. Petrog.*, 79, 5–22,  
540 1999.
- 541 Reinecke, T.: Prograde high- to ultrahigh-pressure metamorphism and exhumation of oceanic  
542 sediments at Lago di Cignana, Zermatt-Saas Zone, western Alps. *Lithos*, 42, 147–189,  
543 doi:10.1016/S0024-4937(97)00041-8, 1998.
- 544 Rolland, Y., Rossi, M., Cox, S.F., Corsini, M., Mancktelow, N., Pennacchioni, G., Fornari, M., and  
545 Boullier, A.M.: <sup>40</sup>Ar/<sup>39</sup>Ar dating of synkinematic white mica: insights from fluid-rock reaction in  
546 low-grade shear zones (Mont Blanc Massif) and constraints on timing of deformation in the NW  
547 external Alps. *Geol. Soc. Spec. Publ.*, 299, 293–315, doi:10.1144/SP299.18, 2008.
- 548 Sartori, M.: *L'unité du Barrhorn (Zone pennique, Valais, Suisse)*. Mémoires de Géologie 6, Lausanne,  
549 Switzerland, 1990.
- 550 Sartori, M., Gouffon, Y., and Marthaler, M.: Harmonisation et définition des unités  
551 lithostratigraphiques briançonnaises dans les nappes penniques du Valais. *Eclogae Geol. Helv.*, 99,  
552 363–407, doi:10.1007/s00015-006-1200-2, 2006.
- 553 Schaer, J. P., Reimer, G.M., and Wagner, G.A.: Actual and ancient uplift rate in the Gotthard region,  
554 Swiss Alps: A comparison between precise levelling and Fission-Track Apatite age. *Tectonophysics*,  
555 29, 293–300, doi:10.1016/0040-1951(75)90154-7, 1975.
- 556
- 557 Schlunegger, F., Burbank, D.W., Matter, A., Engesser, B., and Mödden, C.: Magnetostratigraphic  
558 calibration of the Oligocene to Middle Miocene (30–15 Ma) mammal biozones and depositional  
559 sequences of the Swiss Molasse Basin. *Eclogae Geol. Helv.*, 89, 753–788, 1996.
- 560 Schlunegger, F., and Kissling, E.: Slab rollback orogeny in the Alps and evolution of the Swiss



- 561 Molasse basin. *Nat. Commun.*, 6, 1-10, 8605, doi:10.1038/ncomms9605, 2015.
- 562 Schlunegger, F., Matter, A., and Mange, M.A.: Alluvial-Fan Sedimentation and Structure of the  
563 Southern Molasse Basin Margin, Lake Thun Area, Switzerland. *Eclogae Geol. Helv.*, 86, 717–750,  
564 1993.
- 565 Schlunegger, F., Slingerland, R., and Matter, A.: Crustal thickening and crustal extension as controls  
566 on the evolution of the drainage network of the central Swiss Alps between 30 Ma and the present:  
567 Constraints from the stratigraphy of the North Alpine Foreland Basin and the structural evolution of  
568 the. *Basin Res.*, 10, 197–212, doi:10.1046/j.1365-2117.1998.00063.x, 1998.
- 569 Schmid, S.M., Fügenschuh, B., Kissling, E., and Schuster, R.: Tectonic map and overall architecture  
570 of the Alpine orogen. *Eclogae Geol. Helv.*, 97, 93–117, doi:10.1007/s00015-004-1113-x, 2004.
- 571 Schmid, S.M., Pfiffner, O.A., Froitzheim, N., Schönborn, G., and Kissling, E.: Geophysical -  
572 geological transect and tectonic evolution of the Swiss-Italian Alps. *Tectonics*, 15, 1036–1064,  
573 doi:10.1029/96TC00433, 1996.
- 574 Sinclair, H.D., Coakley, B.J., Allen, P.A., and Watts, A.B.: Simulation of foreland basin stratigraphy  
575 using a diffusion model of mountain belt uplift and erosion: An example from the Central Alps,  
576 Switzerland. *Tectonics*, 10, 599–620, 1991.
- 577 Spear, F.S.: *Metamorphic Phase Equilibria And Pressure-Temperature-Time-Paths* (2nd ed.)  
578 Mineralogical Society of America monograph, USA, 1994.
- 579 Spiegel, C., Kuhlmann, J., Dunkl, I., Frisch, W., Von Eynatten, H., and Balogh, K.: The erosion  
580 history of the Central Alps: Evidence from zircon fission track data of the foreland basin sediments.  
581 *Terra Nova*, 12, 163–170, doi:10.1046/j.1365-3121.2000.00289.x, 2000.
- 582 Spiegel, C., Siebel, W., Frisch, W., and Berner, Z.: Nd and Sr isotopic ratios and trace element  
583 geochemistry of epidote from the Swiss Molasse Basin as provenance indicators: Implications for the  
584 reconstruction of the exhumation history of the Central Alps. *Chem. Geol.*, 189, 231–250,  
585 doi:10.1016/S0009-2541(02)00132-8, 2002.
- 586 Spillmann, P.: *Die Geologie des Grenzbereichs im penninisch-ostalpinen südlichen Berninagebirge*,  
587 Ph.D. thesis, ETH Zürich, Switzerland, 262pp., 1993.
- 588 Spillmann, P., and Büchi, H.: The Pre-Alpine Basement of the Lower Austro-Alpine Nappes in the  
589 Bernina Massif (Grisons, Switzerland; Valtellina, Italy), in: *The Pre-Mesozoic Geology in the Alps*,  
590 edited by von Raumer, J.F. and Neubauer, F., Springer Berlin Heidelberg, Germany, 457–467, 1993.
- 591 Steck, A., and Burri, G.: *Chemismus und Paragenesen von Granaten aus Granitgneisen der*  
592 *Grünschiefer- und Amphibolitfazies der Zentralalpen*. *Schweiz. Miner. Petrog.*, 51, 534–538, 1971.
- 593 Stutenbecker, L., Delunel, R., Schlunegger, F., Silva, T.A., Šegvić, B., Girardclos, S., Bakker, M.,  
594 Costa, A., Lane, S.N., Loizeau, J.-L., Molnar, P., Akçar, N. and Christl, M.: Reduced sediment supply  
595 in a fast eroding landscape? A multi-proxy sediment budget of the upper Rhône basin, Central Alps.  
596 *Sedimentary Geol.*, 375, 105–119, doi:10.1016/j.sedgeo.2017.12.013, 2018.
- 597 Stutenbecker, L., Berger, A., and Schlunegger, F.: The potential of detrital garnet as a provenance  
598 proxy in the Central Swiss Alps. *Sedimentary Geol.*, 351, 11–20, doi:10.1016/j.sedgeo.2017.02.002,  
599 2017.
- 600 Stutenbecker, L., 2019, Detrital garnet chemistry from the Molasse basin. doi:  
601 10.6084/m9.figshare.8269742.v1.
- 602 Thélin, P., Sartori, M., Lengeler, R., and Schaerer, J.-P.: Eclogites of Paleozoic or early Alpine age in  
603 the basement of the Penninic Siviez-Mischabel nappe, Wallis, Switzerland. *Lithos*, 25, 71–88, 1990.



- 604 Tolosana-Delgado, R., von Eynatten, H., Krippner, A., and Meinhold, G.: A multivariate  
605 discrimination scheme of detrital garnet chemistry for use in sedimentary provenance analysis.  
606 *Sedimentary Geol.*, 375, 14–26, doi:10.1016/j.sedgeo.2017.11.003, 2018.
- 607 Trümpy, R.: *Geology of Switzerland. A guide book, Part A: An outline of the geology of Switzerland.*  
608 Basel, Switzerland: Wepf, 1980.
- 609 Vernon, A.J., van der Beek, P.A., and Sinclair, H.D.: Spatial correlation between long-term  
610 exhumation rates and presentday forcing parameters in the western European Alps. *Geology*, 37, 859–  
611 862, doi:10.1130/G25740A.1, 2009.
- 612 Vernon, A.J., van der Beek, P.A., Sinclair, H.D., and Rahn, M.K.: Increase in late Neogene denudation  
613 of the European Alps confirmed by analysis of a fission-track thermochronology database. *Earth  
614 Planet. Sc. Lett.*, 270, 316–329, doi:10.1016/j.epsl.2008.03.053, 2008.
- 615 Wagner, G. A., Reimer, G.M., and Jäger, E.: Cooling ages derived by apatite fission track, mica Rb-Sr  
616 and K-Ar dating: The uplift and cooling history of the central Alps, *Memorie degli Istituti di Geologia  
617 e Mineralogia dell' Università di Padova*, 30, 1–27, 1977.
- 618  
619 Weber, S., and Bucher, K.: An eclogite-bearing continental tectonic slice in the Zermatt–Saas high-  
620 pressure ophiolites at Trockener Steg (Zermatt, Swiss Western Alps). *Lithos*, 232, 336–359,  
621 doi:10.1016/j.lithos.2015.07.010, 2015.
- 622 Wildi, W.: Heavy mineral distribution and dispersal pattern in penninic and ligurian flysch basins  
623 (Alps, northern Appennines). *Giorn. Geol.*, 47, 77–99, 1985.
- 624 Wittmann, H., von Blanckenburg, F., Kruesmann, T., Norton, K.P., and Kubik, P.W.: Relation  
625 between rock uplift and denudation from cosmogenic nuclides in river sediment in the Central Alps of  
626 Switzerland. *J. Geophys. Res. - Earth*, 112, F04010, 1–20, doi:10.1029/2006JF000729, 2007.



627 *Table 1: Sample locations and characteristics of the Molasse sandstones from the Napf fan*

| Sample name | Sampling location    | Lithostratigraphy (Matter, 1964; Schlunegger et al. 1996) | Magnetostratigraphic section (Schlunegger et al. 1996) | Magnetostratigraphic age (Schlunegger et al. 1996) |
|-------------|----------------------|---|--|--|
| LS2017-3    | 47.00566<br>7.971325 | UFM, Napf beds  | Fontannen section                                      | ca. 14 Ma  |
| LS2018-5    | 46.93913<br>7.950800 | UMM, Luzern formation                                     | Schwändigraben section                                 | ca. 19 Ma  |
| LS2016-18   | 46.77463<br>7.732383 | LFM, Thun formation                                       | Prässerebach section                                   | ca. 25 Ma  |





628 *Table 2: Sample locations and characteristics of potential source rocks*

| Sample name | Sampling location   | River catchment                               | Metamorphic grade            | Lithological unit                                     |
|-------------|---------------------|---|------------------------------|---|
| LS2018-12   | 46.72026<br>7.24548 | Ärgera, ca. 30<br>km <sup>2</sup>             | Not metamorphic              | Gurnigel flysch (detrital<br>garnets)                 |
| LS2018-40   | 46.39026<br>8.54124 | Valle di Foioi, ca.<br>3 km <sup>2</sup>      | Alpine<br>amphibolite-facies | Orthogneiss of the Antigorio<br>nappe, Lepontine dome |
| LS2016-43   | 46.43955<br>8.50115 | Valletta di<br>Fiorina, ca. 8 km <sup>2</sup> | Alpine<br>amphibolite-facies | Paragneiss of the Lebendun<br>nappe, Lepontine dome   |



629 *Table 3: Minimum, maximum and average contents (including standard deviation in brackets) of the*  
 630 *five common garnet endmembers in the Molasse sediments. For the full dataset we refer to*  
 631 *Stutenbecker (2019).*

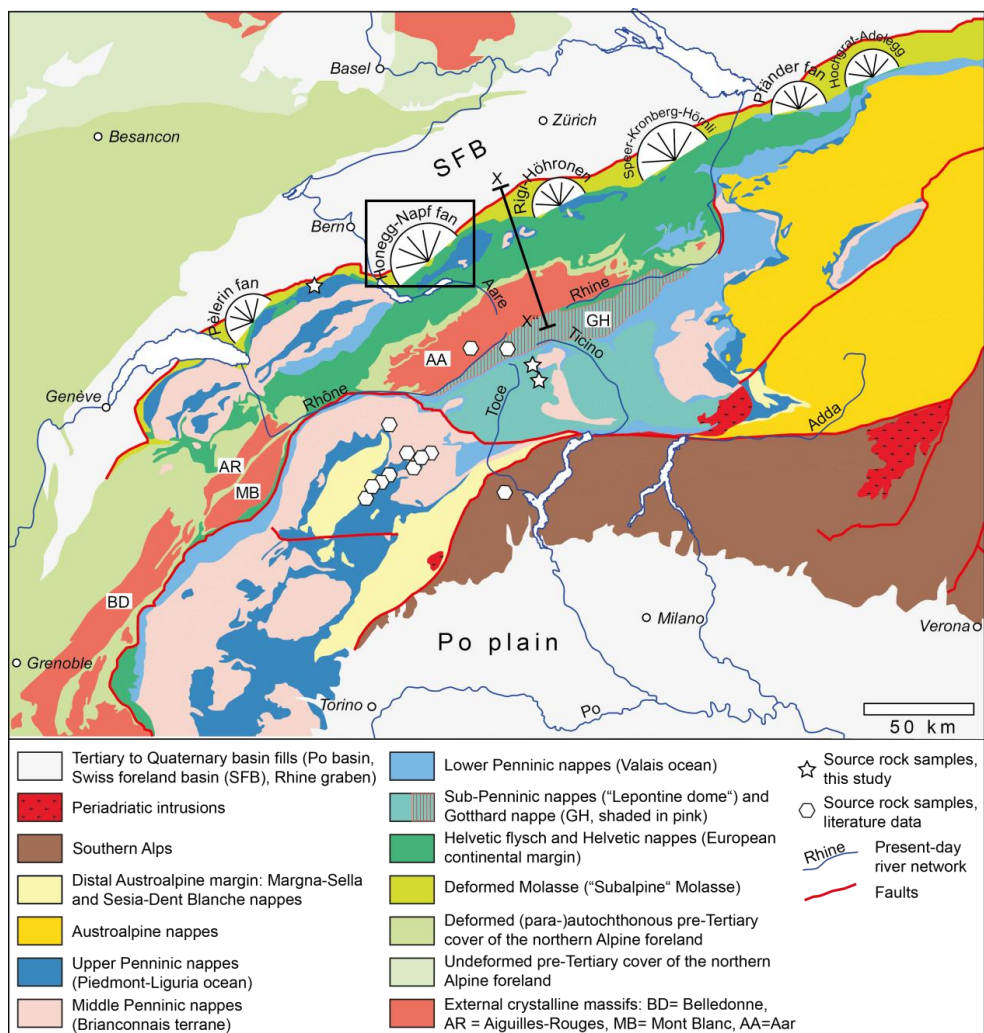
| Sample                | Minimum, maximum and average contents | Almandine (%) | Andradite (%) | Grossular (%) | Pyrope (%) | Spessartine (%) |
|-----------------------|---------------------------------------|---------------|---------------|---------------|------------|-----------------|
| <b>25 My</b><br>n=110 | min                                   | 5             | 0             | 0             | 0          | 1               |
|                       | max                                   | 86            | 48            | 40            | 22         | 38              |
|                       | average (standard deviation)          | 70 (12)       | 2 (5)         | 9 (7)         | 9 (5)      | 9 (8)           |
| <b>19 My</b><br>n=88  | min                                   | 0             | 0             | 1             | 0          | 0               |
|                       | max                                   | 84            | 91            | 55            | 39         | 39              |
|                       | average (standard deviation)          | 65 (16)       | 3 (13)        | 16 (12)       | 9 (8)      | 5 (6)           |
| <b>14 My</b><br>n=77  | min                                   | 24            | 0             | 5             | 0          | 1               |
|                       | max                                   | 74            | 9             | 60            | 26         | 39              |
|                       | average (standard deviation)          | 50 (12)       | 2 (2)         | 32 (11)       | 6 (5)      | 9 (9)           |



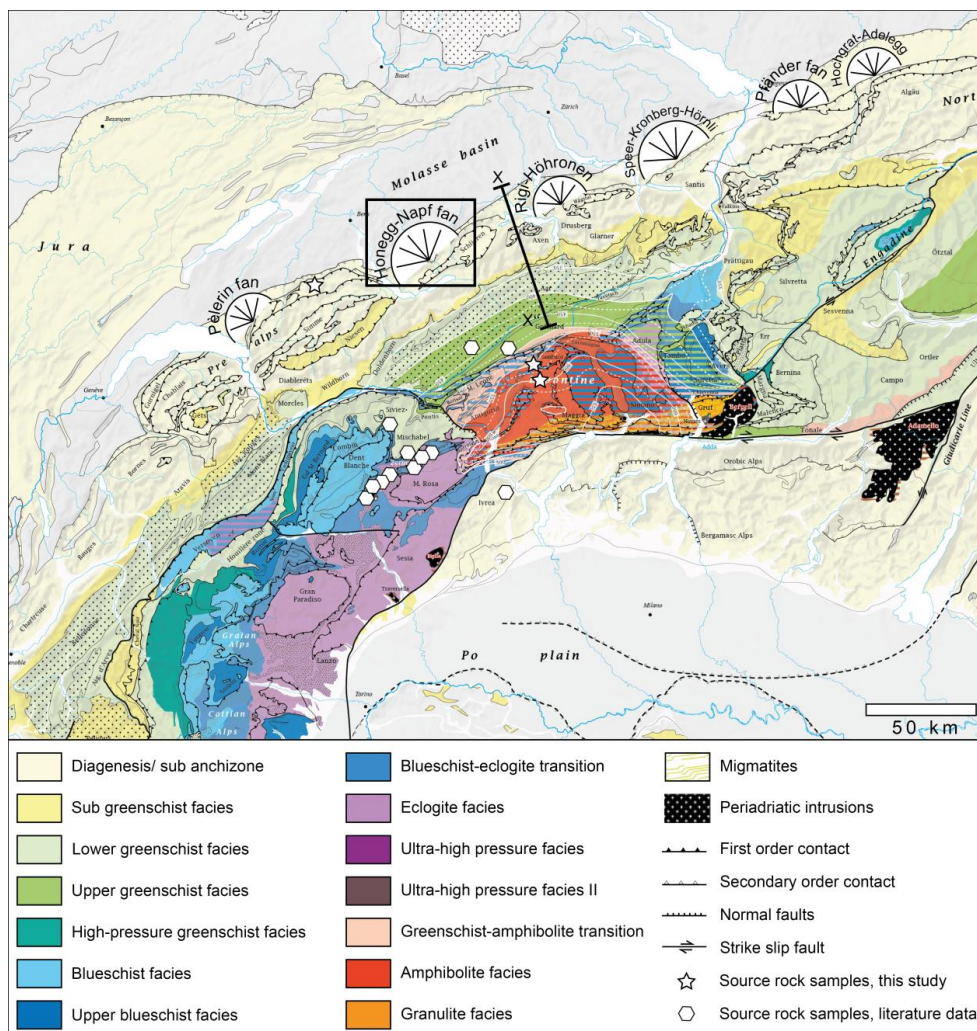
632 *Table 4: Results from classification following Mange & Morton (2007) and Tolosana-Delgado et al.*  
 633 *(2018). Using the linear discriminant method of Tolosana-Delgado et al. (2018) garnets were*  
 634 *attributed to one single class if the probability for that class was  $\geq 50\%$ . Several grains were assigned*  
 635 *mixed probabilities with  $< 50\%$  per class; these are listed separately below.*

| Types after Mange & Morton (2007) | Mange & Morton (2007) |       |       | Classes after Tolosana-Delgado et al. (2018) | Tolosana-Delgado et al. (2018) |       |       |
|-----------------------------------|-----------------------|-------|-------|--|--------------------------------|-------|-------|
|                                   | 25 My                 | 19 My | 14 My |  | 25 My                          | 19 My | 14 My |
| Ci-type (high-grade metabasic)    |                       | 5 %   | 15 %  | Eclogites (Class A)                          |                                | 1 %   |       |
| B-type (amphibolite facies)       | 96 %                  | 84 %  | 80 %  | Amphibolites (Class B)                       | 71 %                           | 81 %  | 78 %  |
| A-type (granulite-facies)         | 3 %                   | 8 %   |       | Granulites (Class C)                         |                                | 9 %   | 5.5 % |
| D-type (metasomatic)              | 1 %                   | 3 %   | 5 %   | Igneous (Class E)                            | 5 %                            | 3 %   | 12 %  |
|                                   |                       |       |       | <i>Mixed probabilities Classes B-C</i>       | 1 %                            | 1 %   |       |
|                                   |                       |       |       | <i>Mixed probabilities Classes A-B-C</i>     |                                | 5 %   | 4.5 % |

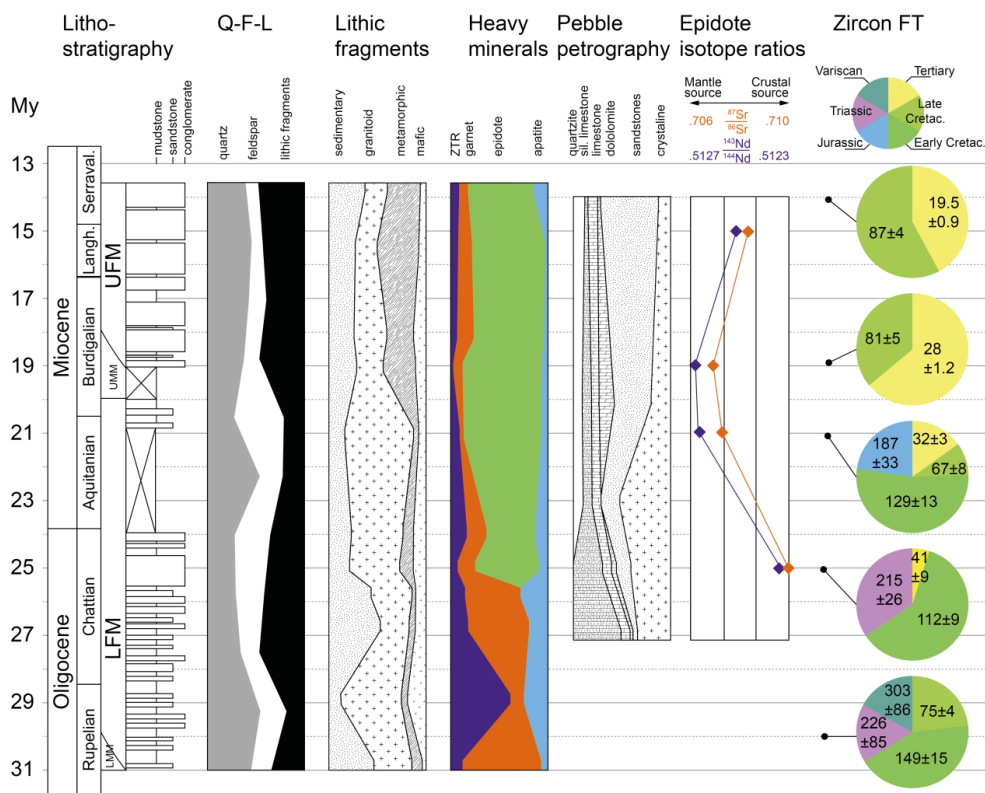
636



637  
 638 *Fig. 1: Simplified tectonic map of the Central Alps after Schmid et al. (2004) highlighting the location of*  
 639 *alluvial fan deposits within the northern alpine foreland basin as well as the most important source*  
 640 *rock units in the hinterland. The Napf fan, marked by the black rectangle, is located in the central part*  
 641 *of the Swiss foreland basin (SFB).*

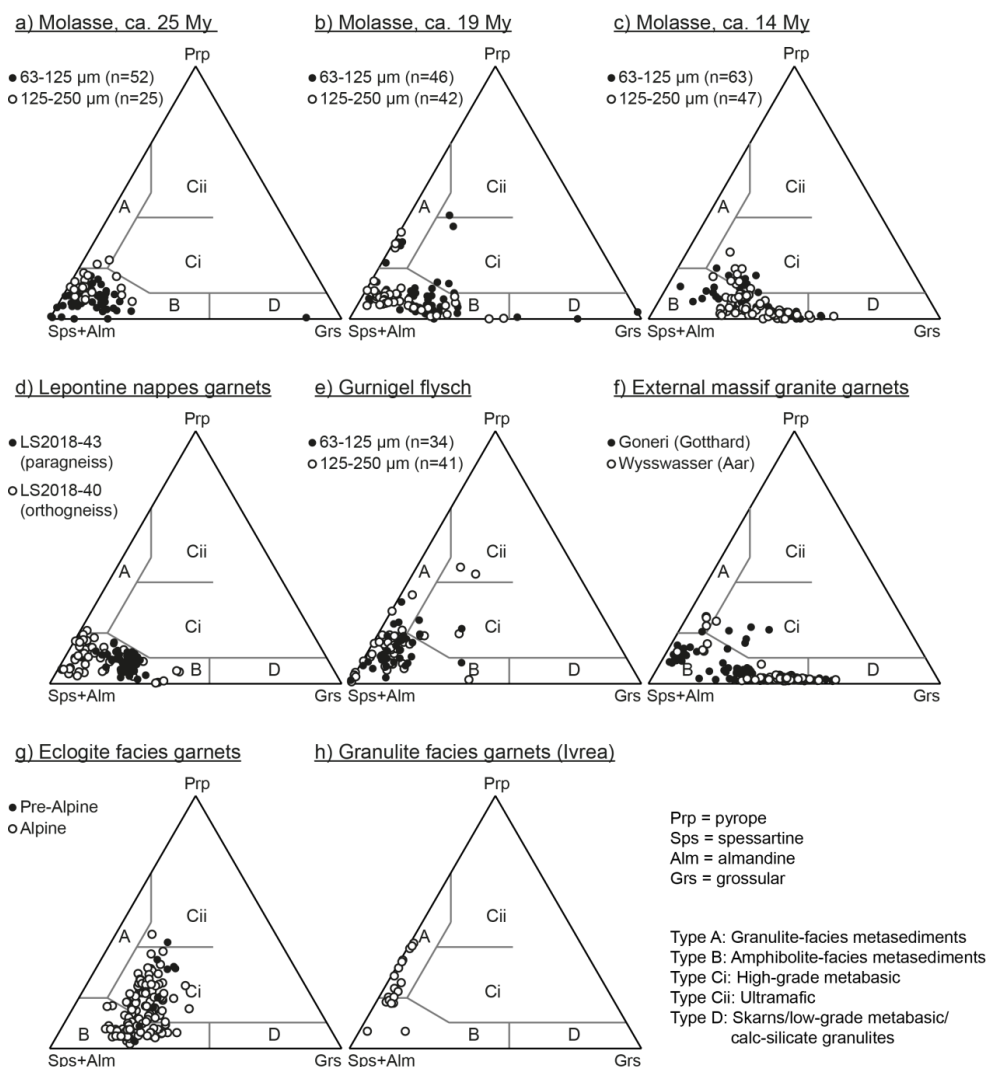


642  
 643 Fig. 2: Metamorphic map of the Central Alps (Bousquet et al., 2012) showing the distribution and  
 644 grade of alpine metamorphism. Note the increase from north to south from lower greenschist- to  
 645 eclogite-facies conditions.



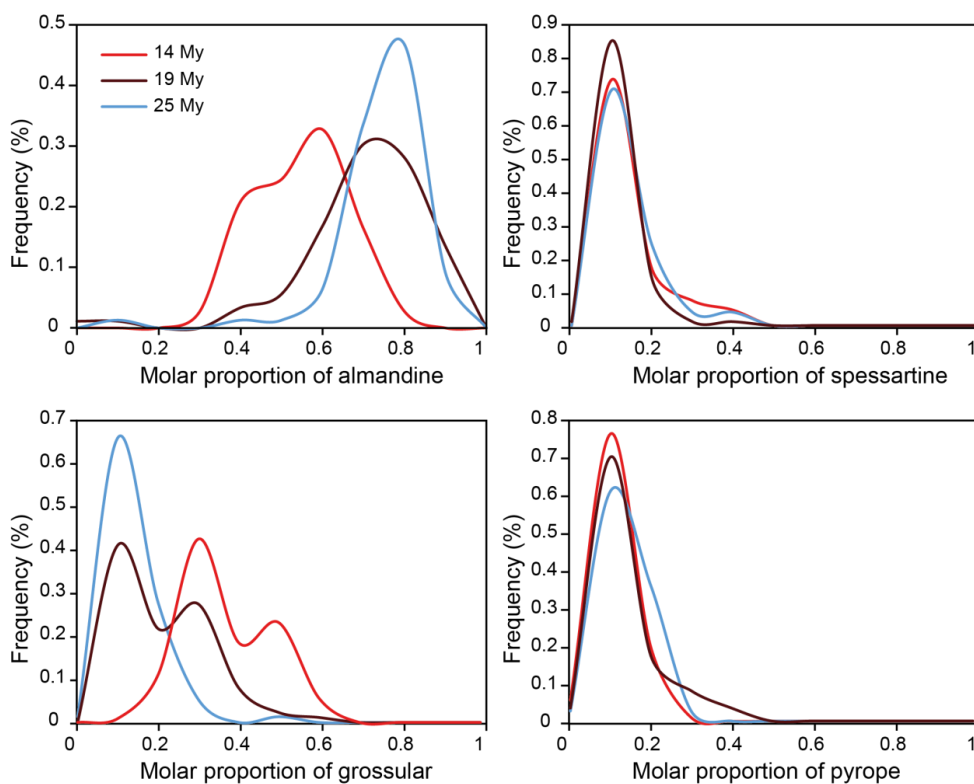
646

647 *Fig. 3: Compilation of published compositional data in the Honegg-Napf fan. Heavy mineral and rock*  
 648 *fragment data from the sand grain size after von Eynatten (2003), pebble petrography after*  
 649 *Schlunegger et al. (1998), epidote isotope ratios after Spiegel et al. (2002) and zircon fission-track*  
 650 *(FT) data after Spiegel et al. (2000).*



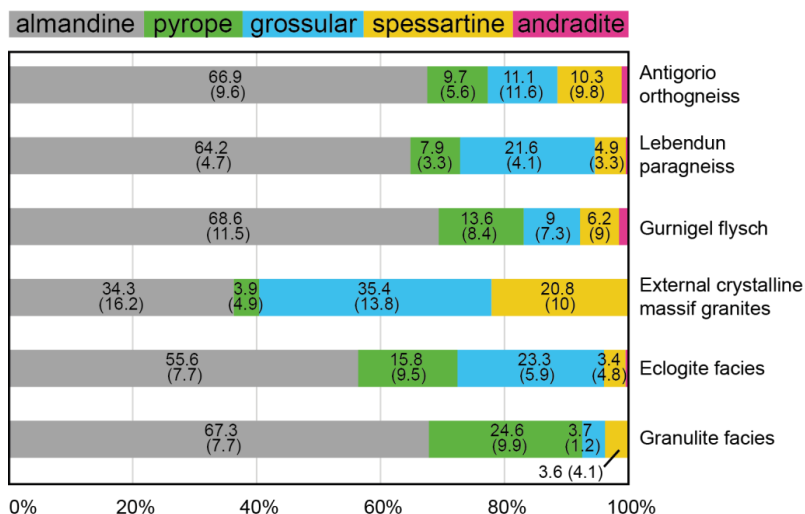
651

652 *Fig. 4: Ternary plots following the classification scheme of Mange & Morton (2007). (a-c) Garnet*  
 653 *provenance changes in Molasse sandstones are marked by an increasing grossular content with*  
 654 *decreasing age. Source rock data from (d) Lepontine gneisses (this study), (e) the Gurnigel flysch (this*  
 655 *study), (f) external massif granitoids (Stutenbecker et al., 2017), (g) eclogite-facies rocks (Chinner &*  
 656 *Dixon, 1973; Ernst & Dal Piaz, 1978; Oberhänsli, 1980; Sartori, 1990; Thélin et al., 1990; Reinecke,*  
 657 *1998; Cartwright & Barnicoat, 2002; Angiboust et al., 2009; Bucher & Grapes, 2009; Weber &*  
 658 *Bucher, 2015), (h) granulite-facies rocks from the Ivrea zone in the Southern Alps (Hunziker & Zingg,*  
 659 *1980).*



660  
661 *Fig. 5: Shift of garnet compositions between the 25 My-, 19 My- and 14 My-old Molasse samples,*  
662 *plotted as relative frequency of the four most common endmembers almandine, grossular, spessartine*  
663 *and pyrope. While spessartine and pyrope contents are similar among the three samples, the*  
664 *proportion of almandine decreases and the proportion of grossular increases with decreasing age.*  
665  
666

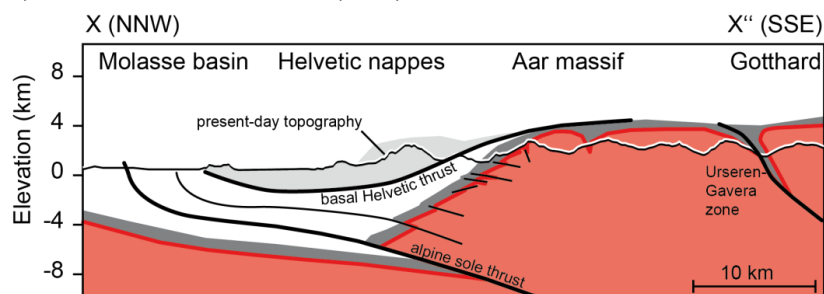




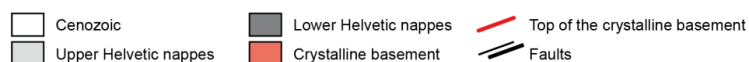
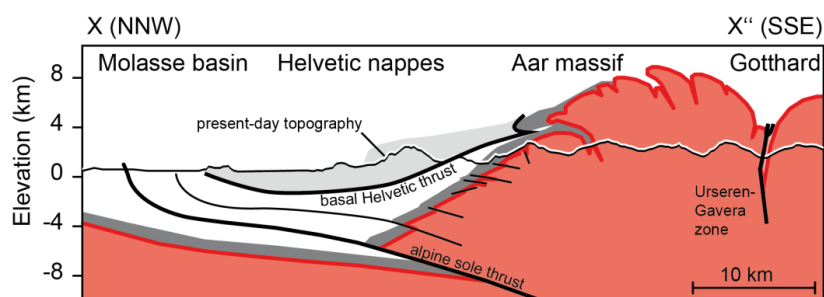
667 0% 20% 40% 60% 80% 100%  
 668 Fig. 6: Average garnet compositions of potential source rocks from the Lepontine nappes (Antigorio  
 669 orthogneiss and Lebedun paragneiss; this study), the Gurnigel flysch (this study), the external  
 670 crystalline massif granites (Stutenbecker et al., 2017), eclogite facies rocks (Chinner & Dixon, 1973;  
 671 Ernst & Dal Piaz, 1978; Oberhänsli, 1980; Sartori, 1990; Thélin et al., 1990; Reinecke, 1998;  
 672 Cartwright & Barnicoat, 2002; Angiboust et al., 2009; Bucher & Grapes, 2009; Weber & Bucher,  
 673 2015), and granulite facies rocks (Hunziker & Zingg 1980). The means and standard deviations (in  
 674 brackets) of each component are given for each bar.



a) Reconstruction after Pfiffner (2017)



b) Reconstruction after Nibourel et al. (2018)



675

676 *Fig. 7: Cross sections from X to X'' through the Aar massif simplified after Pfiffner (2017) and*  
677 *Nibourel et al. (2018). For trace of cross section see Fig. 1. (a): The reconstructed top of the*  
678 *crystalline basement in the Aar massif is located ca. 1-2 km higher than the present-day topography*  
679 *according to Pfiffner (2017). (b): In a revised version by Nibourel et al. (2018) the contact between*  
680 *the basement and the overlying Helvetic cover nappes is reconstructed to be steeper, resulting in ca. 8*  
681 *km of (now eroded) crystalline crust on top of the present-day topography.*